ON RF RESIDUAL LOSSES IN SUPERCONDUCTING CAVITIES

J. Halbritter, IK II
Kernforschungszentrum, Postfach 3640
D 7500 KARLSRUHE, Fed. Rep. Germany

Abstract

Superconducting cavities show temperature independent rf losses ($<10^{11}$Hz) at $T < 2$-4K which are named rf residual losses. In this paper these losses are classified according to their origin: Bulk residual losses - either in the metal or in the dielectrics - can be avoided by proper design and handling of the rf cavities and by proper surface preparations. Interface residual losses cannot be avoided but can be reduced by improving the quality of the metal-oxide interface.

These interface losses are classified according to the density of interface states n_{IS} and rf field component involved in:

Normal conducting losses ($\propto \omega^2 n_{IS} B^2$)
Electric interface losses ($\propto n_{IS} E_\perp^2$)
Diffuse surface scattering ($\propto (n_{IS} E_\parallel)^2$)

These rf losses mechanisms are discussed and compared with experimental results.

I. INTRODUCTION

The rf losses in metal cavities are classified according to the rf field component at the surface - $B_{\parallel}$ or $E_{\perp}$ - causing these losses. The magnetic field $B_{\parallel}(t) = B_{\parallel}\cos\omega t$ yields the rf shielding currents $j(\vec{r},t)$ in the metal causing rf losses P_B, which, for sufficiently plane surfaces, are described by: [1]

$$P_B = \frac{1}{2} \oint ds R_B H_{\parallel}^2 + \frac{\omega\mu_o}{2} \bar{d}_B \oint ds \frac{\mu''}{\mu_r^2} H_{\parallel}^2 \qquad (1)$$

where the integral $\oint ds$ is extended over the cavity surface. The material properties of the cavity wall are included in the surface resistance R_B, which is the real part of the surface impedance $Z_B = E_{\parallel}/H_{\parallel}$ of the transverse wave in the metal. [1] The imaginary part [1,2]

$$\mathrm{Im}Z_B = X_B = \omega\mu_o\lambda_B, \quad \lambda_B = \int_o^\infty dx\; B_{\parallel}(x)/B_{\parallel}(o) \qquad (2)$$

is related to the magnetic field penetrating into the metal ($x \geq 0$). λ_B yields an inductance change, i.e. the cavity eigenfrequency ω increases according to $\Delta\omega = \omega_o X/2G_B$, with $G_B \approx 10\text{-}10^3\Omega$ the magnetic geometry factor. [2]

The second part in Eq.(1) describes the rf losses due to the susceptibility $\mu(\omega) = \mu' + i\mu''(\mu' = \mu_r\mu_o)$ of the dielectric coating of the wall having $\bar{d}_B$ as mean thickness. [1]

P_B - i.e. Z_B and μ - include only losses related to $B_{\parallel}$ and neglect any effect of the longitudinal rf field component $E_{\perp}$. These rf losses P_E are given - like Eq.(1) - by: [1,3]

$$P_E = \frac{1}{2}\frac{\varepsilon_o}{\mu_o} \oint ds\; R_E E_{\perp}^2 + \frac{\omega\varepsilon_o}{2} \bar{d}_E \oint ds \frac{\varepsilon''}{\varepsilon_r^2} E_{\perp}^2 \qquad (3)$$

where R_E is the real part of an electric surface impedance Z_E with an imaginary part - $\omega\mu_o\lambda_E$ with λ_E the electric field penetration depth into the metal. The second part in Eq.(3) describes dielectric losses in the coating of a mean thickness $\bar{d}_E$. Related to $H_{\parallel}$ and $E_{\perp}$ in Eqs. (1) and (3) it should be mentioned, that $H_{\parallel}$ and $E_{\perp}$ differ from cavity fields $H_{\parallel}^C = H_{\parallel}\cdot\mu_r$ and $E_{\perp}^C = E_{\perp}\cdot\varepsilon_r$ due to the shielding by the dielectric coating.

For <u>normal conducting cavities</u>, like Cu, $R_B \gg R_E$ holds and rf losses in dielectric oxide coatings ($d < 10^2$ mm) are negligible. Thus the rf losses are given by $P_B = R_B \oint ds\; H_{\parallel}^2/2$, where R_B is plotted in Fig. 1, yielding rf losses, e.g.,

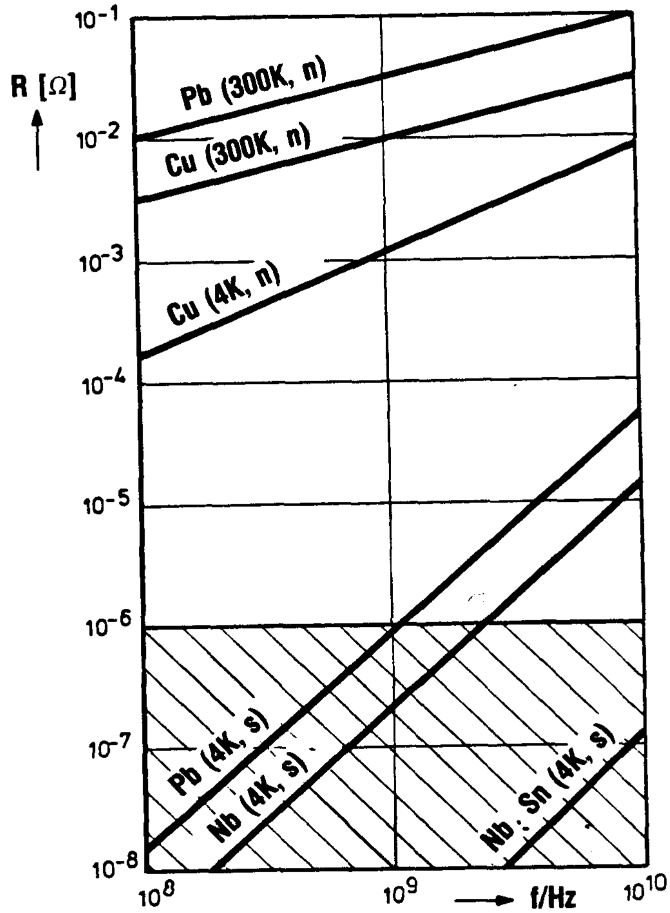

Fig. 1: Surface resistance of pure Pb, Cu, Nb and Nb_3Sn at 300 K and 4 K in the GHz range. The strong reduction of R compared to R(Cu, 4K) is due to the energy gap $2\Delta > 10^{11}$ Hz·h opening in the superconducting state. The shaded region indicates the appearance of additional - residual - losses R_{res}, e.g., due to dust, joints or interface states.

$P_B = 10^{-3}\ \Omega(30\ \mathrm{mT}/\mu_0)^2/2 = 30\ \mathrm{W/cm^2}$. These rf losses cause cooling problems and huge power bills for large rf accelerators. To lower these losses cooling is advantageous because the electron mean free path ℓ is increasing. But at rf frequencies the penetration depth $\lambda_B \propto 1/\sqrt{\omega\ell}$ shrinks only for $\lambda_B \gg \ell$, whereas for $\lambda_B \lesssim \ell$ the anomalous skin effect limits the rf losses to rather high values depicted in Fig. 1 by R(Cu,4K). These rf losses can be lowered further only by using superconducting rf cavities - see Fig. 1. This reduction of R_B by more than 5 orders of magnitude overcompensates the additional costs for He liquification and is thus the reason for the application of superconducting cavities in rf accelerators - see workshop 1980.

The magnetic rf losses in superconductors are strongly temperature dependent and this is quantitatively described by the BCS theory (Figs. 2 and 3):[2,4]

$$R_{BCS}(T,\omega) \cong r_o(\lambda_L,\xi_F,\ell)\ \omega^2 \cdot \exp(-\Delta/kT)/kT\,(\hbar\omega<\Delta/2,\ T\lesssim T_c/2) \qquad (4)$$

with $\Delta_o/kT_c \approx 2$ for Pb, Nb and Nb_3Sn having T_c = 7.2 K, 9.25 K and 18 K.

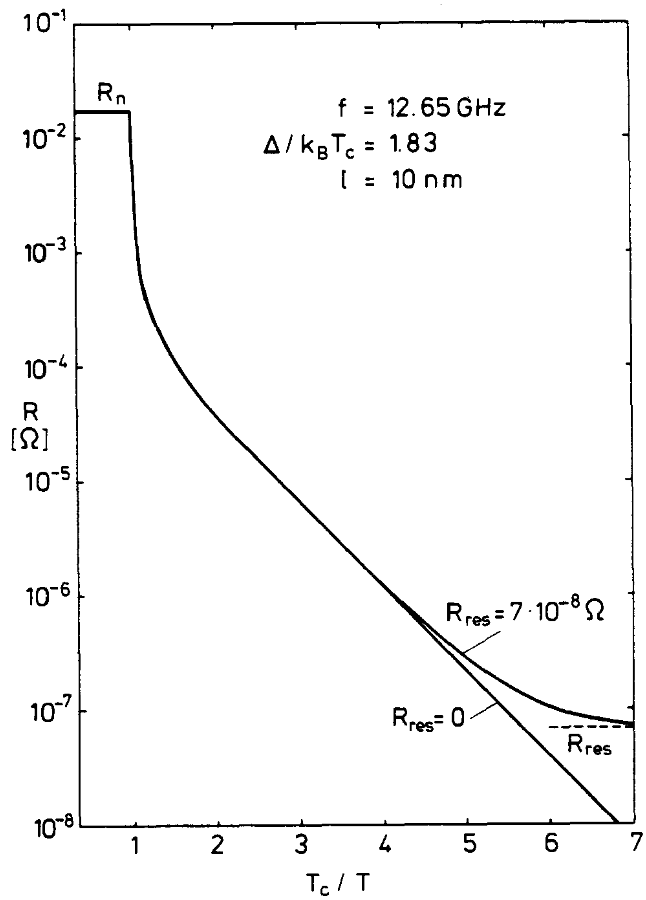

Fig. 2: The temperature dependence of the surface resistance of Nb at 12 GHz. The decrease of R(T) at T_c = 9.25 K is stronger than exponential because the penetration depth $\lambda_B(T \lesssim T_c)$ decreases rapidely also with lowering the temperature. Below about 4 K $\lambda_B(T) \cong$ const holds and thus $R_{BCS}(T) \propto \exp(-\Delta/kT)/kT$ describes the decrease of R(T) till the residual rf losses dominate below 2 K.

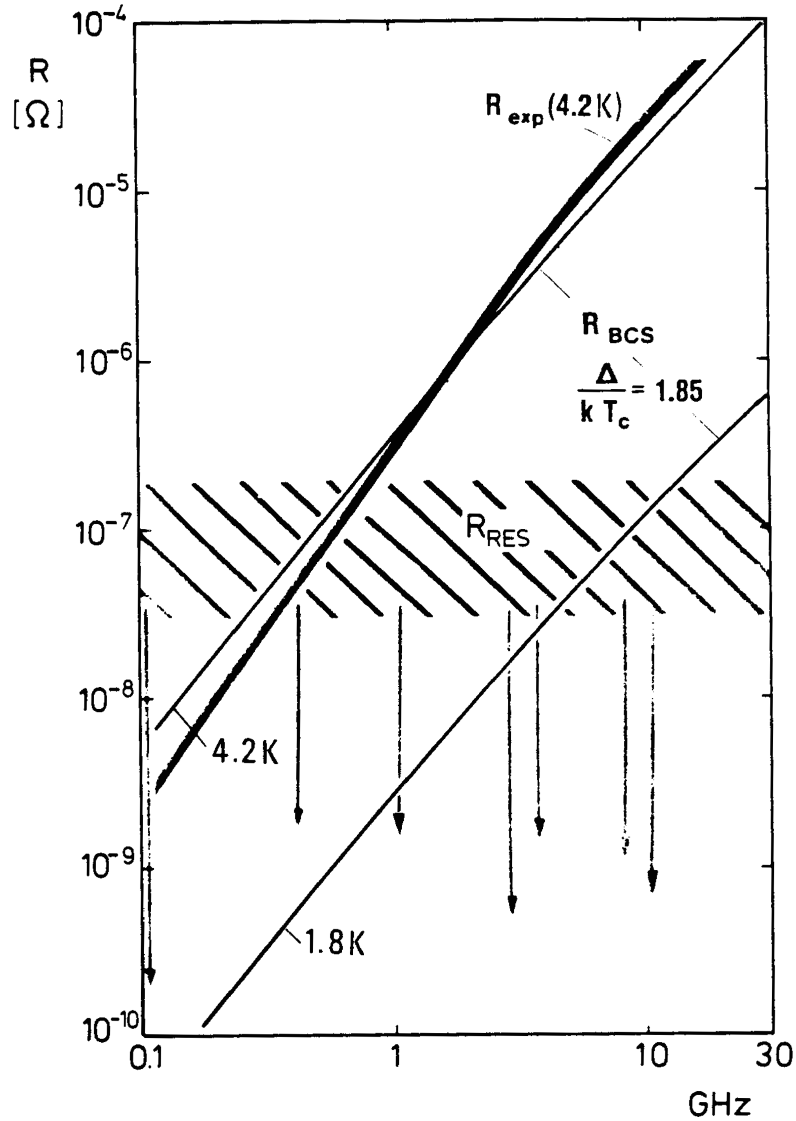

Fig. 3: Summary of experimental (░) and computed (—) surface resistance of Nb between 0.1 and 30 GHz. The R (4.2 K, f) values show a cross over of experimental and computed values due to the smearing of the BCS singularity by O precipitates. The differences of the computed slopes at 4.2 K and 1.8 K are due to $R(T) \propto \exp(-(\Delta + \hbar\omega/2)/kT)/kT$.
The residual rf losses R_{res} show a large scatter depending on cavity design and surface preparation. The arrows (░) indicate best values.

The material parameters of superconductors are $\lambda_L = \sqrt{m/\mu_o e^2 n_c}$ (n_c = density of conduction electrons) as London penetration depth and $\xi_F = \hbar v_F/2\Delta$ as Pippard coherence length. This exponential temperature dependence - see Eq.(1) and Fig. 2 - is levelling off between 10^{-7} and 10^{-9} Ω at the residual surface resistance R_{res}. In Fig. 3 it is shown for Nb, that R_{res} is sensitively depending on surface preparation, where - beside cleanness [5] and being dust free [5,6] - the crucial parameters are discussed below. To explain R_{res} in its dependence on material parameters, several proposals have been given as there are :

- normal conducting inclusions in the superconductor (Part II)
- frozen in magnetic flux (Part III)
- dielectric rf losses (Part IV) and
- interface rf losses (Part.V);

which will be compared with experiments in Part VI.

Since the reviews [7,8] by the author, no systematic studies on R_{res} have been carried out. Hence in Parts II - VI the arguments of Ref. 8 are repeated, but refined and improved by new informations and thus reference is mainly given to papers published 1974 and later.

II. Rf LOSSES OF NORMAL CONDUCTORS IN PROXIMITY WITH SUPERCONDUCTORS

Normal conductors in proximity with superconductors weaken the superconductivity in the superconductor while diffusing superconductivity into the normal conductor. This diffusion $\propto \exp(-|\vec{r}-\vec{r}\,'|/\xi_{GL})$ is governed by the Ginzburg-Landau-coherence length $\xi_{GL} \propto \sqrt{\xi_F \cdot \ell}$ and depends sensitively on the magnetic field and on the temperature.[9-11] Such a dependence in the GHz surface resistance $R(T,B_{rf})$ was found in Nb_3Sn cavities [11] where $\xi_{GL} \approx 3$ nm is rather small and thus small normal conducting inclusions become independently normal conducting at small fields of $B_{rf} \approx 5$mT $<< B_c(Nb_3Sn)$. For Nb $\xi_{GL} > 30$ nm and for Pb $\xi_{GL} > 10^2$ nm hold and thus such [11] $R(T,B_{rf})$ monotonously increasing with B_{rf} have not been observed. The often observed peak structure $R(T,B_{rf})$ in the surface resistance of Nb, where R is decreasing between 1 and 5 mT, [12] has nothing to do with the proximity effect as indicated by the decrease of R with B_{rf}. This feature, being typical for Nb, is explained by localized electron states easily being driven out of equilibrium by rf absorption.[13,14] Such deviations from thermal equilibrium occur also for small ($\lesssim 1$ µm) normal conducting regions embedded in a superconducting matrix There the decrease of surface resistance of the normal conductor corresponds to a dc resistance decrease of up to 6 orders of magnitude [9]. These deviations from thermal equilibrium have important implications for the rf breakdown in superconducting rf cavities [13].

III. Rf LOSSES CAUSED BY FROZEN-IN MAGNETIC FIELDS

Cooling rf cavities through the critical temperature T_c in an ambient magnetic field B_{dc} freezes in magnetic flux in the superconductor, depending on demagnetization factor at T_c and cooling rate.[8,15] For composit materials, like Cu-Pb or Nb-Nb_3Sn, temperature gradients around the highest T_c cause thermoelectric current, generatign frozen-in flux.[15,16] Neglecting details discussed in Refs. 15 and 17, these losses are given by:

$$R_B \cong \frac{B_{dc}}{B_c(0)(1-(T/T_c)^2)} R_n(\omega) \qquad (5)$$

where B_{dc} is either the external - earth - field at T_c or a mean field caused, e.g., by thermo-electric currents. For Nb, and thus also for Nb_3Sn, below about 1 GHz R_B increases with B_{rf} quite strongly due to fluxoids dynamics,[15] and shows a specific temperature dependence.[17]

As a guide for Nb cavities cooled in 0.05 mT (earth field)

$$R_B(0.05\ \mathrm{mT}) \approx 10^{-6}\ \Omega \sqrt{f/\mathrm{GHz}} \qquad (5')$$

can be used[15]. This indicates the need of proper magnetic shielding of superconducting rf cavities to approach $R_{res} < 10^{-6}\Omega$.

IV. ELECTRIC AND MAGNETIC RF LOSSES IN DIELECTRICS

These rf losses are described by Eqs. (1) and (3) and have a frequency and temperature dependence given by $\varepsilon'(\omega,T)$ and $\mu'(\omega,T)$ or $tg\delta_E = \varepsilon'/\varepsilon''$ and $tg\ \delta_B = \mu'/\mu''$. As shown in Fig. 4, $tg\ \delta_E \lesssim 10^{-5}$ increases with temperature for $T \gtrsim 4.2$ K but decreases with frequency for $\omega \geq 10^8$ Hz for amorphous dielectrics. For dielectrics containing dipols rf losses are larger.[18,19] For well annealed, clean Al_2O_3 $tg\delta_E \cong 4\cdot 10^{-8}$ has been achieved at He-temperatures[20]. For superconducting rf cavities the losses can be estimated by (Eq. (3)):[21]

$$R_E^D = \omega\mu_o\bar{d}_E \frac{tg\delta_E}{2\cdot\varepsilon_r} = \frac{f}{\mathrm{GHz}}\ \frac{\bar{d}_E}{\mathrm{nm}}\ \frac{tg\delta_E}{\varepsilon_r\cdot 10^{-5}} \cdot 4\cdot 10^{-11}\ \Omega \qquad (6')$$

Because of $tg\delta_E < 10^{-5}$ and $\varepsilon_r \gtrsim 10$ for natural, microcristalline amorphous oxide coatings small rf losses-corresponding to $R_E^D \lesssim 10^{-12}\Omega$ - are caused by this loss mechanism. For CO_2 and N_2 $tg\delta_E(\approx 10^9\mathrm{Hz}, \lesssim 4.2\mathrm{K}) \approx 10^{-5}$ holds,[22] thus these losses are negligible.

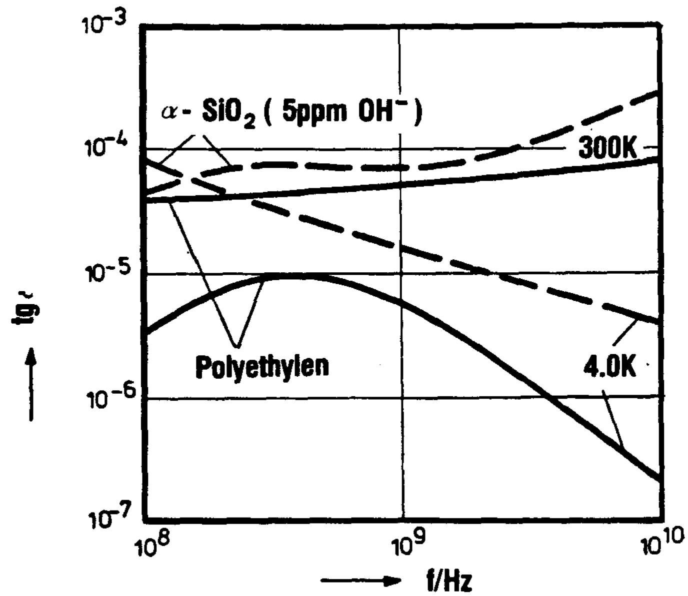

Fig. 4: Dielectric losses of amorphous dielectrics in the GHz range as described by the loss tangent $tg\delta_E = \varepsilon''/\varepsilon'$

Magnetic rf losses in dielectrics are usually negligible. But some dielectrics contain magnetic moments, e.g., Cr in Al_2O_3 [19] or condensed O_2 - N_2 (air). [22] For impurity containing Al_2O_3, tg $\delta_B \lesssim 10^{-5}$ has been observed at 10^8 Hz declining with frequency. [19] Whereas at 4.2 K condensed O_2 has a tg $\delta_B \cong 10^{-4}$, condensed air has a tg δ_B up to $6 \cdot 10^{-3}$ as measured in Ref. 22. Hence condensed air has to be avoided in superconducting rf cavities as shown by (Eq.(1)) [22]

$$R_B^D = \omega\mu_o\bar{d}_B \frac{tg\ \delta_B}{2\ \mu_r} = \frac{f}{GHz}\ \frac{\bar{d}_B}{nm}\ \frac{tg\ \delta_B}{\mu_r \cdot 10^{-5}} \cdot 4 \cdot 10^{-11}\Omega \qquad (6'')$$

because $\mu_r \cong 1$ has to be assumed.

Beside oxide coatings, cavity surfaces are usually contaminated with dust, [6] which shows rf losses described by Eqs.(6') and (6"). Beside these "dielectric or magnetic" rf losses, cristalline dust in the "switched on" state [6] contains electrons in the conduction band being accelerated by $E_\perp(t)$. As shown by the field emission current and by the luminiscence observed, [6] these rf losses are quite large and localized at cavity regions with high $E_\perp$ coinciding with plane cavity parts, where dust sticks best.

V. RF INTERFACE LOSSES

As a definition, these - temperature independent - rf losses are neither bulk dielectric losses, which have been discussed in Part IV, nor shielding current losses in metals, which have been discussed in Parts I and II. Such interface losses may occur [23] due to an enhanced structural disorder in the dielectric adjacent to the metal, but such enhanced disorder seems unlikely in microcristalline amorphous oxide coatings. In contrast electronic disorder adjacent to the metal is much more likely and more effective in causing losses as will be discussed below. This is due to the fact, that the high defect density of amorphous oxides close to metals include also a high density of localized electron states $n_\ell(x,E_F) > 10^{17}/\mathrm{cm}^3$ eV, which hybridize with the high density of conduction electrons $n_c \gtrsim 10^{22}/\mathrm{cm}^3$ eV forming interface states n_{IS}, [3,8,24-26] as shown in Fig. 5.

The wave function of interface states (IS) is given by [24,27]

$$\psi_{IS} = a(E)\psi_\ell + \int dE' \, b(E') \, \psi_c(E') \tag{7}$$

where ψ_ℓ is the wave function localized at V_ℓ - see Fig. 5 - and ψ_c are those of conduction electrons in the metal. In Eq.(7) a(E) is given by $a(E) = c/\sqrt{\pi}/(E-\varepsilon_\ell - \delta\varepsilon_\ell + i\Delta_\ell(E))$ with $|c| = 1$ as phase factor, ε_ℓ as the energy of

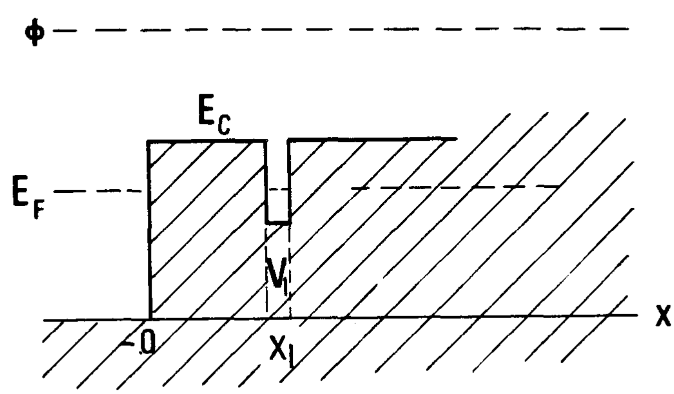

Fig. 5: Potential simulating a dielectric coating (E_c = lower edge of conduction band) on a metal, housing a localized state at x_ℓ. ϕ is the electron affinity of the metal having E_F as Fermi energy.

the localized state, $\delta\varepsilon_\ell$ its shift due to hybridization and $\Delta_\ell(E,x) \cong \Delta_\ell(E)\exp(-2\kappa x)$ with $\kappa = \sqrt{2m(E_c-E_F)}/\hbar$ as attenuation constant. It should be mentioned that $\Gamma(x) \propto \exp(-\kappa x)$ of Refs. 25 and 26 is, in general, too large [24] and has to be substituted by $\Delta_\ell(x) \propto \exp(-2\kappa x)$. Due to the localized part ψ_ℓ, IS shows a stronger electron phonon coupling than ψ_c, approaching the interaction Hamiltonian $H_o \cong 1\text{eV}$ in dielectrics. [26] These IS become also superconducting with an energy gap Δ_{IS}. [25,27] For localized electron pairs in the oxide, which are, e.g., in Nb_2O_5 the dominant defect, [14] at the localized site the unshielded Coulomb repulsion U_{eff} acts on the electrons causing pair weakening. [25] This pair weakening reduces Δ_{IS} so that in a distance $\gtrsim 0.5$ nm $\Delta_{IS} \cong 0$ holds. [26] IS's show an enhanced coupling to the electric field $E_\perp(x,t)$, because $E_\perp(x)$ changes due to shielding by IS's allowing so an enhanced coupling to the electromagnetic rf field. [26]

IS's mediate in two distinctly different ways the interaction of rf field with phonons, namely by a transfer of photons ($\hbar\omega$, $\hbar k$) and by a transfer of electron momenta $\Delta p(t)$ by diffuse surface scattering.

a) Absorption of photons $\hbar\omega$:

These absorption processes in homogeneous metals by $E(x,t)$ have been discussed in Refs. 3 and 4. These losses are described by surface resistances [3,4] $R_B \cong \omega\mu_o\lambda_B\alpha_B$ or $R_E \cong \omega\mu_o\lambda_E\alpha_E$ with λ the penetration - interaction - depth and α a factor describing the absorption process being about 1 for normal conductors. Because then $\lambda_B(10^9\text{Hz}) \gtrsim 1\mu\text{m}$ and $\lambda_E(< 10^{13}\text{ Hz}) < 0.1$ nm holds, electric losses are negligible. In superconductors for $\hbar\omega < \Delta$ (Eq.(4)) α_B and α_E decrease exponentially ($\propto \exp(-\Delta/kT)$). Thus for superconductors for $\hbar\omega < \Delta \simeq h\ 10^{10}$ Hz only normal conducting interface states yield residual losses. Using $n_\ell(\approx 1\text{ nm}) \cong$ $\cong 10^{21}/\text{cm}^3$ for Nb_2O_5 [14] n^n_{IS} ($\gtrsim .5$ nm) $\lesssim 2\cdot 10^{15}$ $\text{cm}^2\cdot(\ell/\text{nm})^3$ holds. These IS inside the Nb energy gap resonantly absorb photons and transfer the energy to phonons. Because of the large transition dipol moment via $E_\perp(x,t)$, this yields mainly $R_{resE} \propto n^n_{IS}$. According to Ref. 26, this yields:

$$\varepsilon_r^2\, R_{resE} \approx 10^{-8}\ \Omega \qquad (8)$$

Whereas above the electric dipol moment was coupling to IS, $E_\perp(x,t)$ changes also the potential energy of localized states allowing transitions between metal and localized site. This process has been discussed in Ref. 3 and becomes small due to the opening of the energy gap of a superconductor.

If the density of IS with $\Delta_{IS} = 0$ is high enough, like in Nb_3Sn with $\ell \approx 1$ nm [11] or in Nb with a damage layer of NbO caused, e.g., by radiation, [14] residual losses given by

$$R_{resB} = (E_{\parallel}/H_{\parallel})^2 d_n \sigma_n = (\omega\mu_o\lambda_B)^2 d_n \sigma_n \tag{9}$$

occur. [26] In Eq.(9) n^n_{IS} are described by the equivalent thickness d_n and conductivity σ_n. Because of the small density n^n_{IS}, their plasma frequency is reduced accordingly. This allows surface plasmon type excitation in the GHz range and thus enhanced electrical residual losses in a similar way as in surface enhanced Raman scattering (SERS): [26]

$$R_{resE} \approx \omega\mu_o d_n \tag{9'}$$

b) Electromagnetic Generation of Ultrasonic Waves

The electromagnetic generation of phonons by rf waves is well understood. [28-32] This - transversal - phonon excitation mechanism include [28-32],as volume parts, the momentum transfer by impurity scattering (collision drag force), which is counteracted by the direct force $qE(t)$ on the ions and,as surface force,the momentum transfer by diffuse surface scattering. The latter dominates in the GHz range [29,30] because of the small penetration depths or film thicknesses used. In Refs. 33 the bulk forces on the ions ($\propto qE(\vec{r},t)$) have erroneously [8,28] been proposed as explanations for R_{res} and for phonon generation. By correctly including the counteracting collision drag force [8,28] the bulk forces exciting phonons become small, especially for short mean free paths ℓ.

The surface force F_s due to diffuse scattering can be described by [32] the momenta $\Delta p = \int dt eE$ of electron,hitting the surface,being transfered there to the atoms. For ideal smooth surfaces,this yields $\Delta p_{\parallel}(t) = eE_{\parallel} \min(\ell, \lambda_B)/\upsilon_F$ and $F_s = -\frac{1}{2}E_{\parallel}(t)$ $n_c \min(\lambda_B,\ell)$.

The transfer process will actually be mediated via the localized part of interface states n^*_ℓ and thus the conversion efficiency α "rf - phonons", i.e. the residual rf losses are described by:

$$R_{resB} \cong \left(e\mu_o\omega \frac{\lambda_B(T)\min(\ell, \lambda_B(T))}{\upsilon_F} n_\ell^*\right)^2 \frac{1}{\rho\upsilon_T} \tag{10}$$

where ρ is the density and υ_T the transversal sound velocity. For normal conductors $\ell << \lambda_B$, this ℓ dependence has been proven as shown in Fig. 6, where the efficiency

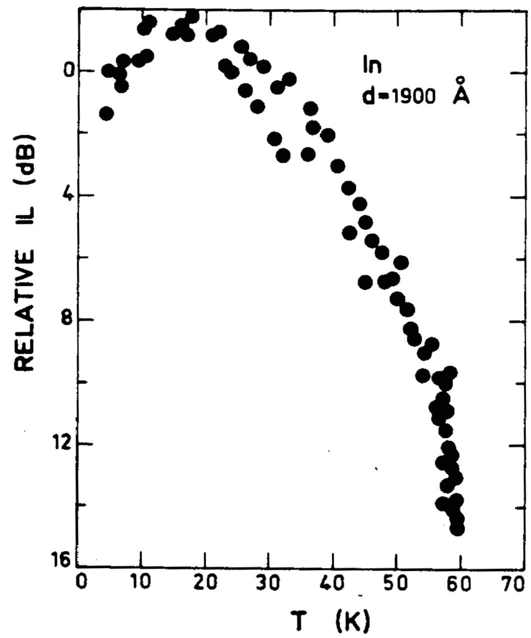

Fig. 6: Experimental [30] temperature dependence of the squared conversion efficiency α^2 (in dB) relative to its value at 4.2K for an indium film.

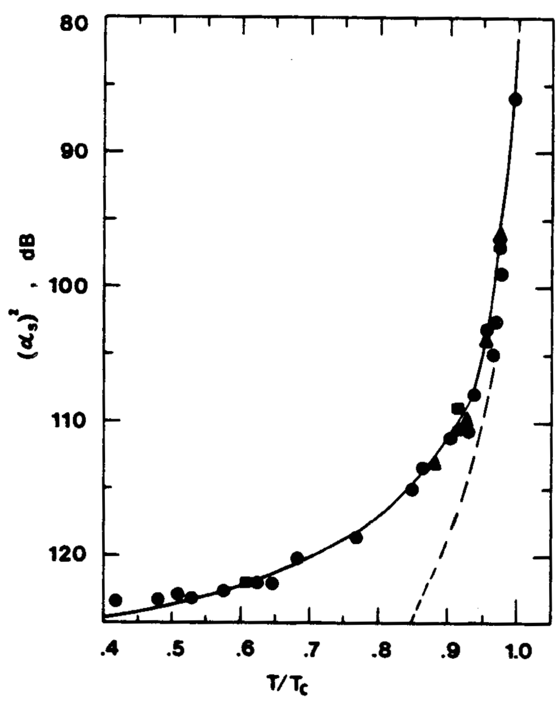

Fig. 7: Measured conversion efficiency squared α_S^2 versus reduced temperature T/T_c for a superconducting In film (T_c=3.4 K). The theoretical curve (—) describes [29] the experimental data well assuming diffuse surface scattering for the whole wave function. The dashed curve (---) assumes diffuse surface scattering for the normal component $n(T)/n_c \cong (1-(T/T_c)^4)$ only and cannot describe the experimental results.

decreases with increasing temperature because ℓ decreases. For superconductors $\lambda_B(T) \lesssim \ell$ holds in the In film shown in Fig. 7 and thus $R_{res} \propto \lambda^4(T)$ is obtained in agreement with Eq.(10). This $R_{res} \propto (\lambda_B(T) \min(\lambda_B(T),\ell))^2$ dependence shows that F_s is not a result of individual single electron scattering events. Instead, as shown in Ref. 28 for bulk scattering, F_s is due momentum transfer by scattering of the overall wave function, i.e. due to weakly localization, and thus not dissappearing in the superconducting state - see Eq. (10). These phonons have been recently detected in ac Josephson junctions.[34]

As indicated by the dependence of $R_{res} \propto n_\ell^{*2}$ and by enhancements of the momentum transfer by roughnesses, R_{resB} will depend on interface quality, i.e. on IS. The phonon detection measurements, where metallic films were evaporated in moderate vacuum onto - contaminated - Si surfaces indicate total diffuse surface scattering.[29,30] This absence of specular reflection yields for $Nb\text{-}Nb_2O_5$ interfaces:

$$R_{resB} \lesssim 5 \cdot 10^{-7}\ \Omega\ (f/GHz)^2 \tag{10'}$$

Obviously improved interface quality, i.e. a reduction of n_{IS} will reduce R_{resB} accordingly.

VI. EXPERIMENTAL RESULTS AND DISCUSSION

Before discussing residual rf losses in the "strict interface sense" outlined in Part V, temperature independent rf losses being bulk in nature and which can clearly be identified or avoided are discussed first.

VI. 1 Bulk Residual Rf Losses

a) Rf losses caused by dust

As summarized in Part IV, dust not only causes rf losses according to its dielectric or magnetic properties but also the dissipation of quasifree electrons of dust in the "switched-on state" yields large rf losses [6] observable, e.g., as emission of light. Dust is usually found at horizontal bottom surfaces below, e.g., a coupling port or a beam hole.[35,36] Such surfaces show enhanced losses together with enhanced electron emission and enhanced radiation damage.[35,36] The amount of dust can be reduced by assembly [5] in dust free methanol or water. Thus, the experimental results of Karlsruhe discussed below are measurements of such "clean" surfaces, and $R_{res} \lesssim 10^{-9}\ \Omega$ have been achieved.

b) Dielectric or magnetic losses in oxides and adsorbates

For Pb the microcristalline PbO has a thickness below 2 nm and Nb is coated by microcristalle amorphous Nb_2O_{5-y} in a thickness below about 3 - 5nm. [14] The adsorbates coating the oxides consists mainly of H_2O and hydrocarbons having a thickness below 0.5 - 2nm, depending on conditioning. [6,14]

As shown by measurements of anodized Nb, these "natural" surfaces have residual losses below 10^{-10} Ω, or $Q_o > 10^{12}$ correspondingly.

Vacuum failures with cold rf cavities yield air condensates which become measurabel ($Q_o \gtrsim 10^{10}$) above 10nm thickness. [22] Heating the cavity to room temperature and pumping the condensates away restaurates the results, if dust is not involved.

c) Rf losses due to frozen-in magnetic flux

Rf losses due to frozen-in magnetic flux are described by Eq.(5) $R_B \propto R_n B_{dc}/B_o$ estimated for Nb by:

$$R_B(0.05\text{ mT}) \approx 10^{-6}\Omega \sqrt{f/\text{GHz}} \qquad (5')$$

B_{dc} is externally applied or caused by thermoelectric currents. The latter are large in composit materials as Pb-Cu, Nb-Cu, Nb_3Sn-Nb, ... As discussed in Part III, these fluxoid rf losses show specific B_{rf}, f and T dependencies and, thus, can be identified.

VI. 2 Interface residual rf losses

The actual interface rf losses can be classified according to the size and the density of defects. Macroscopic defects are oxide filled joints or oxide filled deep fissures. The microscopic defects are given by the density n_ℓ of localized states in front of the superconductor. With decreasing density n_ℓ these residual losses are classified in "normal conducting losses, " , "resonant absorption of $\hbar\omega$ by IS" and momentum transfer by diffuse surface scattering.

a) Oxide filled slits

A typical example for such defects are joints, where two oxidized superconducting surfaces are squeezed together. These two metal surfaces with oxides in between allow strip line modes [7] with wave lengths $\lambda_v \gtrsim 10^{-3}$ cm radiating energy from the cavity into the cold vaccum. This radiation and the residual losses at the poor, metal oxide interfaces because of squeezing, yield large residual losses:[7,8]

$$R_{res} \propto \omega^2$$

Experimentally, such enhanced losses have often been observed: A systematic frequency dependence is shown in Fig. 8,[7] qualitatively thermal resistors at joints often show enhanced rf losses.

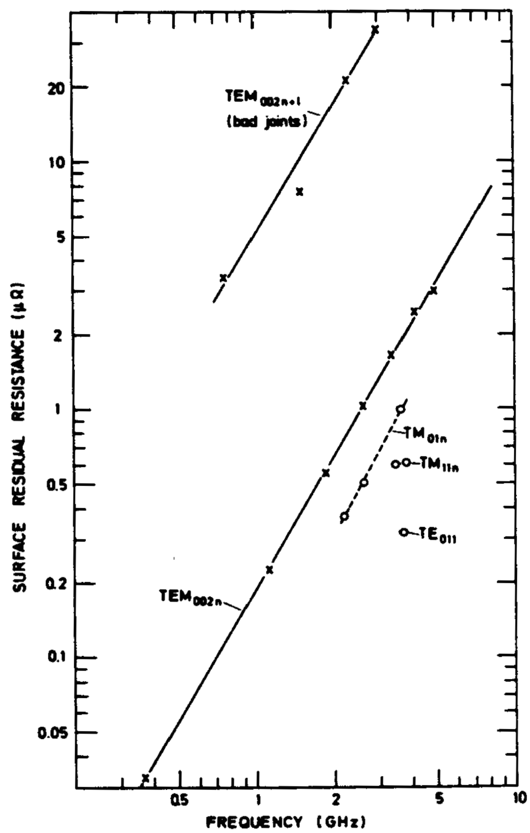

Fig. 8: Surface residual resistances R_{res} of lead plated Cu cavities:[7]
x = TEM harmonics,
o = different modes in one cavity.
In TEM_{002n+1} modes the maximum current is flowing across the joint, whereas in TEM_{002n} modes the current is small. The lowered R_{res} values in the o-cavity
37
are due to an improved joint construction.

b) Normal conducting interface layer

A high density of n_ℓ yields interface states n_{IS} with $\Delta_{IS} \approx 0$ and metallic like conduction. Because of the short mean free path $\ell \approx 0.5$ nm involved, proximity effect stabilizes this superconductivity only up to $B_{rf} \approx$ mT. That is, these "normal conducting regions" yield with B_{rf} decreasing $R(B_{rf})$ values [11]. Because of the strong localization of these states, they are more strongly coupled to phonons and thus deviations from thermal equilibrium are unlikely. [13] As discussed above, these losses are described by

$$R_{resB} \cong (\omega\mu_o\lambda_B)^2 \sigma_n d_n \qquad (9)$$

The losses $R_{resB_1} \cong (\omega\mu_o\lambda_B)^2\sigma_n d_n$ have been identified for Nb3Sn cavities,[11] yielding $d_n \approx 1$ nm for $\sigma_n^{-1} \approx 130$ µΩm. These losses did not depend on Nb_3Sn grain size ($\gtrsim$ 1µm) and thus precipitates at the Nb_3Sn - (Nb_2O_5 SnO_2) interface with T_c*<1 K are the most likely explanation. [11]

The above mechanisms are also appropriate to explain the large residual losses ($\bar{R}_{res} \lesssim 10^{-5}$ Ω) of cold worked Nb or radiation damaged Nb. Cold worked Nb shows, beside $\bar{R}_{res} \lesssim 10^{-5}$ Ω, as outstanding feature the enhanced O concentration in a Nb surface layer (>1 µm)[9,14], which is partly precipated in large lumps of sizes above 10 - 100 nm with $T_c^* \cong 7$ K. [9] The author proposes, that aside from these $T_c^* \cong 7$ K lumps, $T_c^* < 1$ K lumps exist. These lumps are most likely the NbO_x nuclei, which occur at defects of Nb or along Nb grainboundaries. Assuming $\sigma_n^{-1} \approx 200$ µΩcm for these $R_{res} \approx 10^{-5}$ Ω lumps yields $d_n \approx 10$ nm hinting to lumps extending deep into Nb like the $T_c^* \cong 7$ K lumps [9]. This fits to cold working and explains that stress annealing reduces these R_{res} values by about 1 to 2 orders of magnitude.

The electron impact on Nb-Nb_2O_5 interfaces enhances $\bar{R}_{res}$, e.g., from $7 \cdot 10^{-9}$ Ω to $1.8 \cdot 10^{-8}$ Ω at 3.7 GHz. [35] Assuming 1 cm² damage area this yields as local value $R_{res} \lesssim 5 \cdot 10^{-6}$ Ω and thus $d_n \lesssim 10$ nm. This is in line with observations, that stripping of about 10 nm Nb restores [35,36] the previous results. The stoichometry is likely NbO_x produced by electron impact (≈ 1C/cm²) onto the interface. [14]

c. Electrical interface rf losses

For clean metal surfaces the electric losses are with [3] $R_E(\mathrm{GHz}) \approx 10^{-12}$ Ω negligible small. As discussed above interface states enhance R_E by several orders of magnitude, because n_{IS} locally yields a small surface plasma frequency. Thus [3] $R_{resE} \lesssim \omega\mu_o d_n$ with $d_n \cong 0.5$ nm seems plausible for Nb-Nb_2O_5 interface yielding [3] with $\varepsilon_r(4.2\mathrm{K}) \approx 30$

$$R_{resE} \cong 2\pi \cdot 10^{-6} \Omega/\varepsilon_r^{\,2} \cong 2\pi \cdot 10^{-9} \Omega \qquad (9')$$

Such electrical rf losses are difficult to seperate from R_{resB} (Eqs.(9)) and from losses caused by dust. Independent of this problem of separation the diminish of $R_B \propto \omega^2$ with lowering the frequency causes R_{resE} to dominate below 1 GHz - see Fig. 3. This effect is especially prominent in accelerator cavities, where the electric geometry factor G_E is small. This the more as in such cavities [36] dust is easily switched on, which then causes large electric rf losses. [6]

The cavity type allowing to separate electric losses from R_B are reentrant, narrow gap (d_g) cavities because their electric geometry factor $G_E \cong \omega\mu_o d_g/2$ becomes small compared to G_B. Then $P_E = R_E/G_E$ dominates with a frequency dependence $P_E \propto G_E^{-1} \propto 1/\omega$, which has been found experimentally for $d_n < 10^{-3}$ m. [3,38] So recent 10µm gap Nb cavities showing $Q_o > 10^7$ yield [38]

$$R_{resE} \cong 10^{-8}\ \Omega$$

which is in fair agreement with the above (Eq.(9')) estimate and with the difference of R_{res} in TE and TM modes shown in Fig. 8.

d) RF losses by diffuse surface scattering

The momentum transfer by diffuse surface scattering yields, in the sense of the collision drag effect, phonon excitation which can be estimated by Eq.(10):

$$R_{resB} \lesssim 5 \cdot 10^{-7}\ \Omega\ (f/\mathrm{GHz})^2 \qquad (10')$$

where the upper limit occurs for smooth surfaces with a high defect density n_{IS}, i.e. bad Nb_2O_{5-y} quality occuring for, e.g., cold worked or fine grain ($\lesssim$10 nm) Nb. [14]

For Pb cavities, Eq. (10') describes Fig. 8 well, indicating a high n_ℓ concentration. Likely, the now improved Pb plating [39] techniques will result in reduced R_{res} values.

For Nb cavities $R_{res} \propto \omega^{1-2}$ dependencies have been observed in mode families[5,40] fitting to Eq.(10') if R_{resE} by dust and interfaces is taken into account. A clear $R_{res} \propto \omega^2$ dependence with the forfactor given in Eq.(10') as upper limit has been obtained [41] for dust free, plasma oxidized Nb. Because these Nb films have a grain size of 10 nm and are full of defects and because of the plasma oxidation these oxides contain a high defect density n_ℓ and thus R_{res} (Eq.(10')) is at its upper limit [14].

The dependence of n_{IS} and n_{ℓ} on surface preparation and "impurities" has been discussed in length in Ref. 14. Thus here only the main consequences relevant for R_{res} of Nb are presented without repeating all arguments and references of Refs. 8 and 14. For R_{res}, n_{IS}, i.e. localized states n_{ℓ} at E_F, are important. In Nb_2O_5 these localized electron states are oxygen vacancies, V_O, which are propulated by an electron pair and neighbored by two Nb^{4+} sites, because Nb_2O_5 consists of $\{NbO_6\}$ octahedra blocks. The density $n_{\ell}(E \approx E_F)$ is enhanced by an enhanced disorder in Nb_2O_5 or by impurities stabilizing V_O sites. Nb_2O_5 grows on single cristal Nb, NbN or NbC more ordered, resulting in reduced n_{ℓ}. This explains, why UHV annealing reduces R_{res}. On the other hand more slowly grown Nb_2O_5 or thin (< 2 nm) Nb_2O_5 coatings contain less n_{ℓ} explaining so the reduction of R_{res} by Nb_2O_5 annealing or for pinched-off cavities. Impurities in Nb_2O_5 stabilizes or destabilizes V_O and, e.g., Nb_3Sn yields because, of $Sn^{4+}V_OSn^{4+}$ large R_{res} values, whereas N^{3-} in Nb_2O_5, e.g. from quench cooling with N_2, destabilizes V_O and reduces R_{res}. On thin ($\lesssim$1 mm) Nb_2O_5 gases can chemisorbe, where electronic states at E_F enhance R_{res} drastically according to Eq.(10), in line with observations.[42]

Defects in Nb causing $n_{\ell}(Nb_2O_5)$ are related also to H,O,N or C precipitates in Nb surface layers, which precipitates below 700°C.[14] Thus impurities in Nb, the pick-up of impurities and their precipitation should be avoided. For the first demand you need money and a producer. The last two demands are fullfilled by quench cooling the Nb cavities in UHV furnaces, e.g., by N_2 convection cooling at $T \lesssim 600°C$. This should improve the Nb_2O_5 quality in addition by a thin NbN layer and by N^{3-}, where both reduce the V_O site density, like annealing of Nb_2O_5 at 80°C in modest vacuum.[14]
The role of H is often discussed, but never clear evidence for a deterioration[43] of R_{res} was shown for H contents below 10 At%, which are easily achieved by an UHV anneal around 1000°C. This is explained by the fact that these low H-concentration are removed from the surface (> 10² nm) by O precipitates;[14] whereas higher concentrations yield NbH precipitation causing surface defects.

VII SUMMARY

As shown by the above analysis, wet assembly with dustfree agents and a cavity design avoiding joints are crucial, to approach the low R_{res} values, which are mainly caused by partly localized electronic states at the metal oxide interface.

This interface is improved by reducing the defect density in the oxide, which are partly caused by defects of the metal, as discussed in Ref. 14. In the case of Nb this reduction is achieved by stress annealing in an UHV furnace and by reducing the amount of dissolved impurities, which tend to precipitate.

References

1. L.D. Landau, E.M. Lifshitz, Lehrbuch der theoretischen Physik-Elektrodynamik der Kontinua, Kap. 10 (Akademie-Verlag, Berlin, 1967).
2. J. Halbritter, thesis (Universität Karlsruhe); the computer program to obtain R and λ in the frame work of the BCS theory is given in report: KfK extern 3/70-6 (Kernforschungszentrum, Karlsruhe, 1970).
3. J. Halbritter, Z. Phys. B31 (1978) 19.
4. J. Halbritter, Z. Phys. 238 (1970) 466; and 266 (1974) 209.
5. P. Kneisel thesis - KfK - 1645 (Kernforschungszentrum Karlsruhe, 1972) P. Kneisel, O. Stoltz, J. Halbritter, IEEE Trans. NS-18 (1971) 158.
6. J. Halbritter, IEEE Trans. EI-18 (1983) 253.
7. J. Halbritter, J. Appl. Phys. 42 (1971) 82.
8. J. Halbritter, IEEE Trans. MAG-11 (1975) 427.
9. W. Schwarz, J. Halbritter, J. Appl. Phys. 48 (1977) 4618.
10. G. Fischer, R. Klein, phys. kondens. mat. 7 (1968) 7; S.C. Harris, Proc. R. Soc. Lond. A 350 (1967) 267.
11. P. Kneisel, O. Stoltz, J. Halbritter, IEEE Trans. MAG-15 (1979) 21.
12. P. Kneisel, O. Stoltz, J. Halbritter, Low Temperature Physics - LT - 13 (Eds. E. Timmerhaus et al., Plenum Press, 1973) Vol 3, 202.
13. J. Halbritter, Proceedings of the Workshop on Rf superconductinvity Karlsruhe, November 1980 (Kernforschungszentrum, KfK-report 3019 1980), 190
14. J. Halbritter, KfK - report 3728 (Kernforschungszentrum, Karlsruhe, 1984)
15. B. Piosczyk, P. Kneisel, O. Stoltz, J. Halbritter, IEEE Trans. NS-20 (1973) 108.
16. J.P. Judish, C.M. Jones, F.K. Mc Gowan, W.T. Milner, P.Z. Peebles, Phys. Rev. B 15 (1977) 4412.
17. A. Philipp, K. Lüders, K.D. Kramer, Cryogenics 18 (1978) 641.
18. W. Meyer, Mikrowellen Magazin 1 (1977) 15.
19. P.H. Ceperley, IEEE Trans. NS-18 (1972) 222.
20. L.H. Allen, M.R. Beasley, R.H. Hammond, J.P. Turneaure, IEEE Trans MAG-19 (1983) 1003
21 J. Halbritter, Proc. 7. Intern. Vac. Congr. + 3. Intern. Conf. Solid Surfaces, Wien, 1977 (1977) 2015.
22. B. Piosczyk, thesis KfK-1991 (Kernforschungszentrum Karlsruhe, 1974).
23. S.K. Gupta, V.K. Srivastava, J. Phys. Chem. Solids 38 (1977) 1111.
24. J. Halbritter, Surface Science 122 (1982) 80 and IEEE Trans. MAG-19 (1983) 799.
25. J. Halbritter, Solid State Comm. 34 (1982) 675 and 18 (1976) 1447.

26. J. Halbritter, IEEE Trans MAG-17 (1981) 943 and Physica 108B (1981) 917.
27. V. Kresin, J. Halbritter, Proc. LT-17, Karlsruhe, August 1984 (Eds. U. Eckern et al., North Holland, 1984)
28. K. Scharnberg, J. Appl. Phys. 48 (1977) 3462 and J. Low Temp. Phys. 30 (1978) 229.
29. A. Zemel, Y. Goldstein, Phys. Rev. B7 (1973) 191 and B9 (1974) 1499.
30. Y. Goldstein, S. Barzilai, A. Zemel,Phys. Rev. B10 (1974) 5010.
31. R.L. Thomas, M.J. Lea, E.J. Sendezara, E.R. Dobbs, K.C. Lee, A.M. de Graaf Phys. Rev. B14 (1976) 4889.
32. L.R. Ram Mohan, E. Kartheuser, S. Rodriguez, Phys. Rev. B20 (1979) 3233.
33. C. Passow, Phys. Rev. Lett. 28 (1972) 427; E.P. Kartheuser, S. Rodriguez, Appl. Phys. Lett. 24 (1974) 338 and J. Appl. Phys. 47 (1976) 700.
34. P. Berberich, R. Buemann, H. Kinder, Phys. Rev. Lett. 49 (1982) 1500.
35. C.M. Lyneis, P. Kneisel, O. Stoltz, J. Halbritter, IEEE Trans MAG-11 (1975) 417; P. Kneisel, O. Stoltz, J. Halbritter, J. Appl. Phys. 45 (1974)2302
36. Ph. Barnard, G. Cavallari, E. Chiaveri, E. Haebel, H. Heinrichts, H. Lengeler, E. Picasso, V. Piciarelli, J. Tückmantel, Nucl. Instr. Methods 190 (1981) 257.
37. P. Kneisel, Proc. Joint CERN-Karlsruhe Symposium on Superconducting Separator report 3/69-19 (Kernforschungszentrum, Karlsruhe, 1969)
38. W. C. Oelfke, W.O. Hamilton, Rev. Sci. Instrum. 54 (1983) 410.
39. G.J. Dick, J.R. Delayen, IEEE Trans MAG-19 (1983) 1315.
40. W. Bauer, S. Giordano, H. Hahn, J. Appl. Phys. 45 (1974) 5023; U. Klein, thesis (Universität Wuppertal, 1981).
41. R.F. Broom, P. Wolf, Phys. Rev. B16 (1977) 3100.
42. P.B. Wilson, Z.D. Farkas, H.A. Hogg, E.W. Hoyt, IEEE Trans NS-20 (1973)104
43. S. Isagawa, J. Appl. Phys. 51(1980)6010.

Acknowledgement

The author wants to thank for helpful comments of H. Kinder, K. Scharnberg and P. Kneisel.